View metadata, citation and similar papers at core.ac.uk
brought to you by CORE
provided by University of Liverpool Repository

International Forum on Aeroelasticity and Structural Dynamics
IFASD 2019
9-13 June 2019, Savannah, Georgia, USA

INVESTIGATION INTO GUST LOAD ALLEVIATION USING COMPUTATIONAL FLUID DYNAMICS

Philipp Bekemeyer[1], Reik Thormann[1], Sebastian Timme[1]

[1]University of Liverpool
L69 3GH Liverpool
United Kingdom
philipp.bekemeyer@liverpool.ac.uk

Keywords: Gust Load Alleviation, CFD, LFD, Large Aircraft

Abstract: Gust load alleviation has become an integral part of aircraft design to significantly decrease the impact of atmospheric turbulence on aircraft loads, handling qualities and also passenger comfort. During the design of an active control system, the aerodynamic response of the aircraft subjected to gust encounter and control surface deflection effects needs to be modelled. Current industrial practice is based on low-fidelity linear-potential panel methods which are repeatedly evaluated in frequency domain to obtain so-called frequency response functions. Even though rapid turnaround times are possible, important aerodynamic effects such as shock waves and resulting boundary layer separation which define transonic flow conditions are neglected. Typically, robust and adaptive control laws have been designed to account for the shortcomings of the underlying aerodynamic modelling fidelity. In contrast to this, we present initial results of a basic gust controller while using an enhanced aerodynamic modelling by solving the linearised Reynolds-averaged Navier–Stokes equations in frequency domain. Results are presented both for an aerofoil and a large aircraft configuration near transonic cruise conditions. Control laws derived from different levels of the aerodynamic hierarchy are scrutinised during unsteady simulations of realistic gust-encounter scenarios.

1 INTRODUCTION

Aircraft-gust interaction significantly impacts e.g. structural loading, handling qualities and passenger comfort. Hence, gust load analysis is a key task during design and certification to ensure safety and confirm expected aircraft performance. Moreover, minimizing the impact of gusts by employing an active gust load alleviation system, typically through the use of conventional control surfaces, is an integral part of modern aircraft design [1]. The current industrial practice for designing such controllers is driven by aerodynamic response characteristics provided from low-fidelity models based on linear potential theory, such as the doublet-lattice method (DLM) or the unsteady vortex-lattice method [2]. These aerodynamic methods cannot capture transonic and viscous effects, like re-compression shocks over the wings and their interaction with the boundary layer, which inherently occur for large commercial aircraft due to their transonic speeds. Nevertheless, various systems, currently in operation, have been derived from this low-fidelity approach [3].

A short introduction to the current state-of-the-art of load alleviation including several opportunities and challenges can be found in [1]. The applied control systems typically

aim at reducing loads of critical components by deploying control devices. Due to the larger number of disciplines involved, e.g. rigid-body motion, flexible structures and aerodynamics, the modelling fidelity of each discipline is usually low. To account for the shortcomings of the underlying aerodynamic model in particular, robust [4] and adaptive [5] control laws have been proposed in the past. Following a different approach, an enhanced aerodynamic modelling is proposed herein by deriving aerodynamic characteristics using computational fluid dynamics (CFD).

In the past few years, CFD in the context of loads and aeroelastics has been used to analyse aircraft gust encounters, and examples ranging from simple aerofoils to civil aircraft are available [6–8]. However, solving the fully non-linear, time-dependent Reynolds-averaged Navier–Stokes (RANS) equations as aerodynamic model is computationally prohibitive, not to mention specifically for control law design. However, linearised frequency domain (LFD) methods have proven to retain the accuracy of small-amplitude unsteady RANS at significantly reduced computational cost [9–12]. The governing equations are linearised around an arbitrary non-linear steady state and then solved in the frequency domain. The method has become prominent also for industrial applications to calculate frequency response functions (FRF) with respect to structural degrees of freedom e.g. in the flutter-stability context. More recent developments extended the approach towards responses to gust encounters [13–15] and to investigate shock buffet on wings [16, 17].

Herein, a simple active control law for gust load alleviation is discussed which is entirely derived from linearised CFD computations. High-fidelity FRF for both gust encounter (of static and rigid geometries) and control surface influence are computed and used as input to the control design. Resulting control laws are employed during unsteady time-marching RANS simulations to analyse their effectiveness. Moreover, an equivalent control law derived from a low-fidelity panel method is constructed and compared to the herein presented higher-fidelity approach. Finally, results for a close-to-production aircraft configuration are shown which highlight how changes in vertical force and pitching moment are simultaneously suppressed by deploying ailerons and elevators.

2 THEORY

The governing equations are conveniently written in compact semi-discretised residual form as

$$V\frac{\mathrm{d}\mathbf{w}(t)}{\mathrm{d}t} + \mathbf{R}\Big(\mathbf{w}(t), \mathbf{v}_g(t), \boldsymbol{\delta}_{cs}(t)\Big) = \mathbf{0} \tag{1}$$

The flow solution $\mathbf{w}$ is spatially discretised over the computational domain with associated dual-grid cell volumes contained in the diagonal matrix V. The spatial discretisation of the inviscid and viscous flux integrals is described by the residual vector $\mathbf{R}$. Note that the product of flow solution and temporal change of cell volumes is included in the residual vector for ease of notation. The influence of gust disturbances is given by $\mathbf{v}_g(t)$ whereas control surface deflections are contained within $\boldsymbol{\delta}_{cs}(t)$. Since these control surface deflections can be transformed in a relative change in location $\mathbf{x}$ and velocity $\dot{\mathbf{x}}$ of grid nodes by using mesh deformation techniques, equation (1) can be rewritten as

$$V\frac{\mathrm{d}\mathbf{w}(t)}{\mathrm{d}t} + \mathbf{R}\Big(\mathbf{w}(t), \mathbf{v}_g(t), \mathbf{x}(t), \dot{\mathbf{x}}(t)\Big) = \mathbf{0} \tag{2}$$

The difference between the vector of conservative variables $\mathbf{w}$ and an equilibrium solution $\bar{\mathbf{w}}$, and accordingly for external gust disturbances, grid node location and grid node

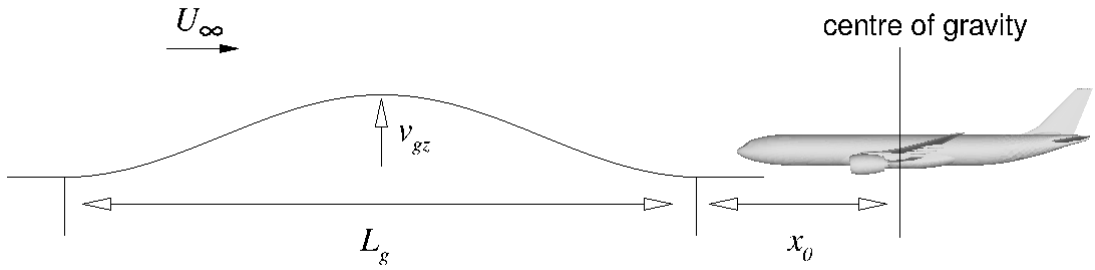

Figure 1: Sketch of gust parameters

velocities, is introduced as

$$\tilde{\mathbf{w}} = \mathbf{w} - \bar{\mathbf{w}} \tag{3}$$

Applying a first-order Taylor expansion while assuming small amplitude harmonic pertubations, equation (2) becomes after some re-arranging

$$\left(\frac{\partial \mathbf{R}}{\partial \mathbf{w}} - i\omega^* V\right) \hat{\mathbf{w}} = -\hat{\mathbf{b}}(\omega^*) \tag{4}$$

with $\hat{\mathbf{w}}$ and $\hat{\mathbf{b}}$ denoting vectors of complex-valued Fourier coefficients. The non-dimensional reduced frequency ω^* is normalized using the reference chord length c_{ref} and the freestream velocity U_∞. Responses to gust and control surface deflections can then be simulated independently, according due to the linearisation assumption, by altering the right-hand side term $\hat{\mathbf{b}}$. For control surface deflections, the right-hand side term becomes

$$\hat{\mathbf{b}}_{cs}(\omega^*) = \left(\frac{\partial \mathbf{R}}{\partial \mathbf{x}} + i\omega^* \left(\frac{\partial \mathbf{R}}{\partial \dot{\mathbf{x}}} + \bar{\mathbf{w}} \frac{\partial V}{\partial \mathbf{x}}\right)\right) \hat{\mathbf{x}}_{cs} \tag{5}$$

with $\hat{\mathbf{x}}_{cs}$ denoting the control surface deflection. For gust responses, we find

$$\hat{\mathbf{b}}_g(\omega^*) = \frac{\partial \mathbf{R}}{\partial \dot{\mathbf{x}}} \frac{\partial \dot{\mathbf{x}}}{\partial \mathbf{v}_g} v_{gz} e^{i(\mathbf{x}+x_0)\frac{\omega^*}{c_{\text{ref}}}} \tag{6}$$

where v_{gz} and x_0 are the vertical gust amplitude and the initial distance between gust and airframe, respectively, as visualised in Figure 1. For a more in-depth discussion of the LFD method, the interested reader is referred to [10, 15].

Once the linearised system is solved at a reduced frequency ω^*, e.g. for the aerodynamic gust response $\hat{\mathbf{w}}_g$, the frequency response function of interest can directly be obtained, e.g. for the change in lift coefficient due to gust excitation, by

$$H_g(\omega^*) = \frac{\partial C_L}{\partial \mathbf{w}} \hat{\mathbf{w}}_g(\omega^*) \tag{7}$$

where $\partial C_L / \partial \mathbf{w}$ is computed explicitly based on the equilibrium solution. Accordingly the pitching moment coefficient and control surface deflections can be analysed.

After discrete FRF are available for all quantities of interest, the simplistic controller enforces that e.g. changes in lift coefficient due to gust $\hat{v}_g$ are counterbalanced by a control surface deflection $\hat{\boldsymbol{\delta}}_{cs}$

$$H_g(\omega^*)\, \hat{v}_g(\omega^*) = -H_{cs}(\omega^*)\, \hat{\boldsymbol{\delta}}_{cs}(\omega^*) \tag{8}$$

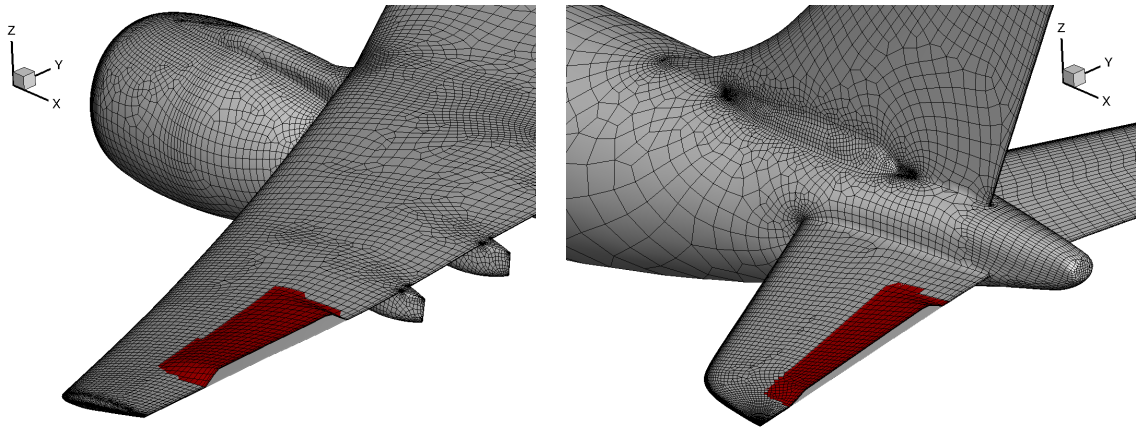

(a) Aileron mode on port side (b) Aileron mode on port side

Figure 2: Aileron and elevator modes for conventional control surfaces of aircraft case.

The FRF of the control law $H_c(\omega^*)$, which describes the necessary control surface deflections to compensate the gust influence, can directly be obtained through rearranging,

$$\hat{\boldsymbol{\delta}}_{cs}(\omega^*) = -H_{cs}^{-1}(\omega^*) \cdot H_g(\omega^*)\, \hat{v}_g(\omega^*) := H_c(\omega^*)\, \hat{v}_g(\omega^*) \tag{9}$$

The control law $H_c(\omega^*)$, which is defined at discrete reduced frequencies, is then transferred into time domain applying a rational function approximation. Herein, the Matlab functionality of the transfer-function estimator *tfest* is used with a fifth-order polynomial. For a system with multiple inputs/outputs of interest, e.g. lift and moment coefficients and aileron and elevator deflections, the control law expression $H_c(\omega^*)$ would have an entry per degree of freedom.

2.1 Practical Implementation Details

The FlowSimulator framework [18] is used to efficiently couple CFD-based aerodynamics with a simple controller. Aerodynamics are solved using the DLR–TAU code which is widely used in the European aerospace sector and validation of the code is available in the literature for steady [19, 20] as well as unsteady cases [20, 21]. The RANS equations in conjunction with the Spalart–Allmaras turbulence model are solved. Inviscid fluxes are discretised applying a central scheme with scalar artificial dissipation. Exact gradients used for viscous and source terms are computed using the Green–Gauss approach. Steady-state solutions are obtained using the backward Euler method with lower-upper Symmetric–Gauss–Seidel iterations [22] and local time-stepping. Convergence is accelerated by applying geometric multigrid and a 2V cycle.

Mesh deformations arising from control surface deflections are calculated with the radial basis function method [23] and assuming blended control surfaces defined by surface modes, as shown in Figure 2 for aileron and elevator of the chosen aircraft case. Gusts are modelled using the field velocity approach which introduces an artificial mesh velocity [24]. The velocity term is added to the governing equations and is prescribed based on the gust excitation while no additional deformation of the computational grid is required. While this preserves the gust shape even for large cells, the influence of the airframe on the gust shape is neglected.

Table 1: Time-domain numerical parameters

Parameter	Aerofoil Case	Aircraft Case
Non-dimensional time-step size	0.1	0.062
Number of time steps	2000	1280
Number of iterations per time step	100	200
Abort density residual	10^{-3}	10^{-8}

Table 2: Frequency-domain numerical parameters

Parameter	Aerofoil Case	Aircraft Case
Number of Krylov vectors	30	100
Number of deflation vectors	10	20
Krylov convergence criterion	10^{-8}	10^{-6}

During unsteady simulations, a dual time-stepping combined with the second-order backward differentiation formula is used, settings of which are summarised in Table 1. Time-step size and number of time steps follow from numerical experiments [15].

The LFD formulation is based on a first-discretise-then-linearise, matrix-forming approach with an analytical, hand-differentiated fluid Jacobian matrix. A generalised conjugate residual solver with deflated restarting is used to solve arising linear systems [25], as defined in equation (4). For preconditioning a block incomplete lower-upper factorisation of the Jacobian matrix with zero level of fill-in is applied [26]. The chosen number of Krylov and deflation vectors together with the linear convergence criterion are given in Table 2 and follow previously published results [15, 25].

3 RESULTS

This section presents results to showcase the performance of the controller derived from a higher-fidelity aerodynamic model. Gust responses for an aerofoil at transonic speeds are first analysed and results are compared between the uncontrolled system, the herein proposed controller and an equivalent DLM-based controller. Afterwards a large civil aircraft, namely the XRF1, is investigated to outline the simplicity of the methodology when moving towards large-scale, industry-relevant test cases.

3.1 NACA0012 Aerofoil

Results are first presented for a NACA0012 aerofoil at weak transonic flow conditions with a freestream Mach number of 0.75 and a chord Reynolds number of 10 million. The angle of attack is set to zero degrees. The computational mesh consists of 70,000 points. The chosen control surface is a flap with the hinge axis located at 75% chord length as shown in Figure 3(a) together with the mesh around the aerofoil. During unsteady simulations mesh deformation techniques are applied to model deflections. The reference steady-state surface pressure distribution in Figure 3(b) gives a symmetric flow field with a very mild shock at roughly 20% chord length.

As a prerequisite to the gust load alleviation controller, FRF are computed for the flap as well as the gust response at 21 reduced frequencies uniformly spaced in the interval $[0, 1]$. The corresponding function H_c of the control law to compensate for the change in lift coefficient is presented in Figure 4. Note that the FRF include both the gust

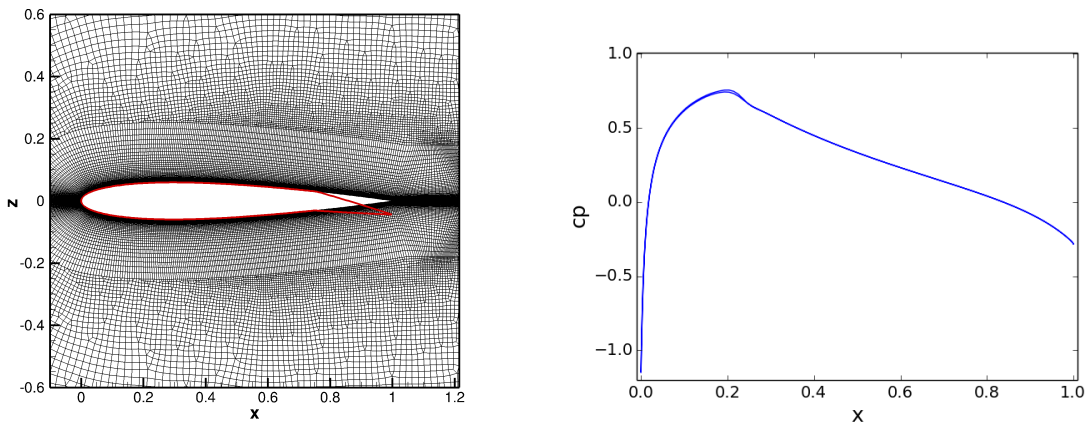

(a) Mesh around aerofoil and control surface

(b) Surface pressure distribution

Figure 3: Mesh around aerofoil, control surface definition (in red) and steady-state pressure coefficient for NACA0012 aerofoil case.

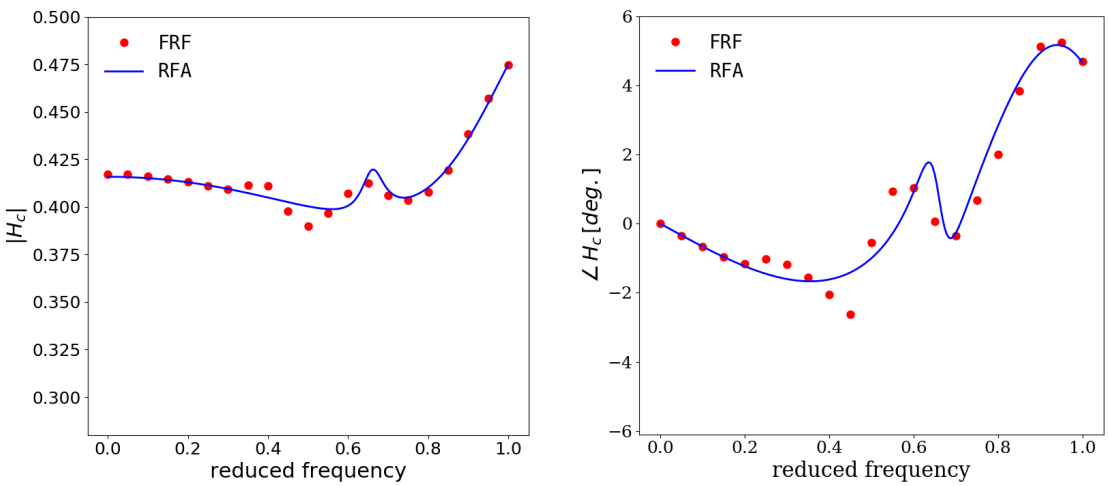

(a) Magnitude

(b) Phase

Figure 4: Frequency response function H_c and its rational function approximation for NACA0012 aerofoil.

and flap influence resulting in a clearly non-linear behaviour especially around a reduced frequency of 0.5. As outlined in Section 2, a rational function approximation (RFA) is used to transfer the discrete frequency-domain FRF into time domain, thus enabling its inclusion in a time-marching unsteady RANS simulation. The resulting fifth-order polynomial after optimizing the coefficients is also given in Figure 4 showing overall good agreement albeit some deviations for the magnitude and phase in the highly non-linear response range. Higher-order polynomials have been tested but have not been found to be beneficial due to overfitting and/or increased complexity.

Afterwards, the controller is incorporated in an unsteady RANS gust response simulation to investigate its effectiveness for non-small gust amplitudes which violate the modelling assumptions of the underlying LFD method. The sensor, necessary for the basic feed-forward control, is arbitrarily positioned at two chord lengths upstream of the aerofoil. Figure 5(a) shows the time history of the lift coefficient response for a long 1–cos gust with non-dimensional gust length of 32 and a maximum gust velocity of 6.6% of the

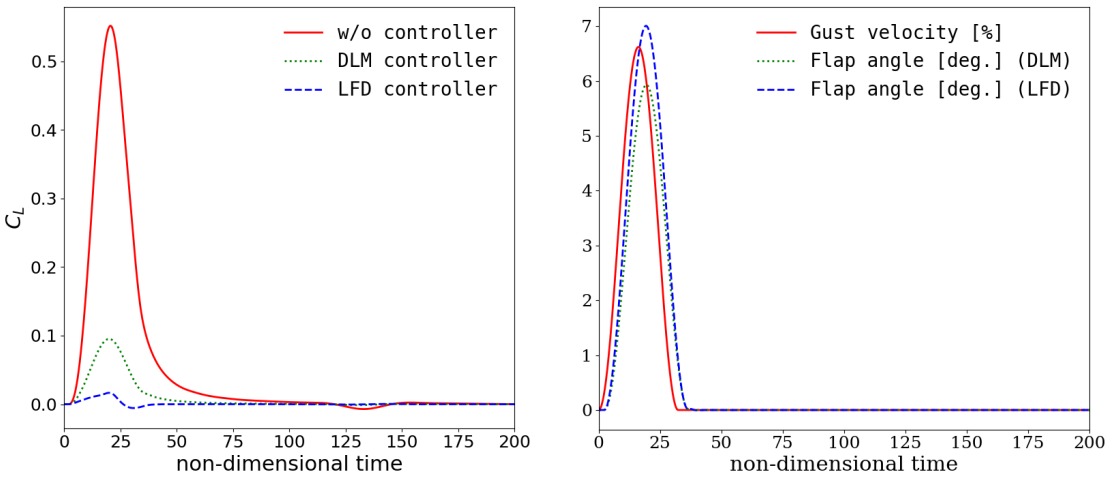

(a) Lift coefficient response

(b) Gust velocity and flap angle

Figure 5: Aerofoil results with and without control for dimensionless gust length of 32.

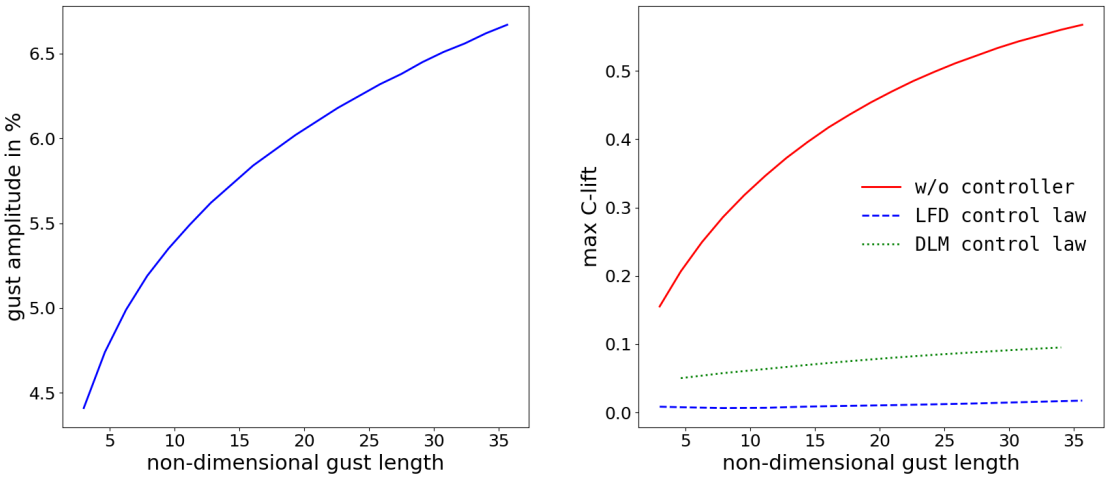

(a) Vertical gust amplitude over gust length

(b) Maximum lift coefficient

Figure 6: Gust amplitude and maximum lift response with and without control for aerofoil case

free-stream velocity. Even in this non-linear regime with transient flow separation and reattachment, the controller based on linearised aerodynamics significantly reduces the lift response. Only a minor lift build-up can be observed around a non-dimensional time of 21 coinciding with the location of the maximum lift of the uncontrolled system response. The time signal of the gust velocity at the sensor as well as the obtained flap angle are presented in Figure 5(b). Since the sensor is placed upstream of the aerofoil, a phase lag is needed for the flap angle while the general shape is similar to the gust excitation with a maximum deflection of 7.05 deg. Altering the sensor position would result in a shift in phase lag but retain the overall efficiency of the control system.

A more classical DLM-based controller has also been derived following the aforementioned sampling and RFA approach. The lift coefficient response to the same gust as before utilising the lower-fidelity controller is also shown in Figure 5(a). Even though the maximum lift coefficient is reduced by approximately a factor of 5.5 compared to the uncontrolled system, the RANS LFD-based controller performs significantly better especially around the non-dimensional time of 23. This is primarily due to the overestimation of the control

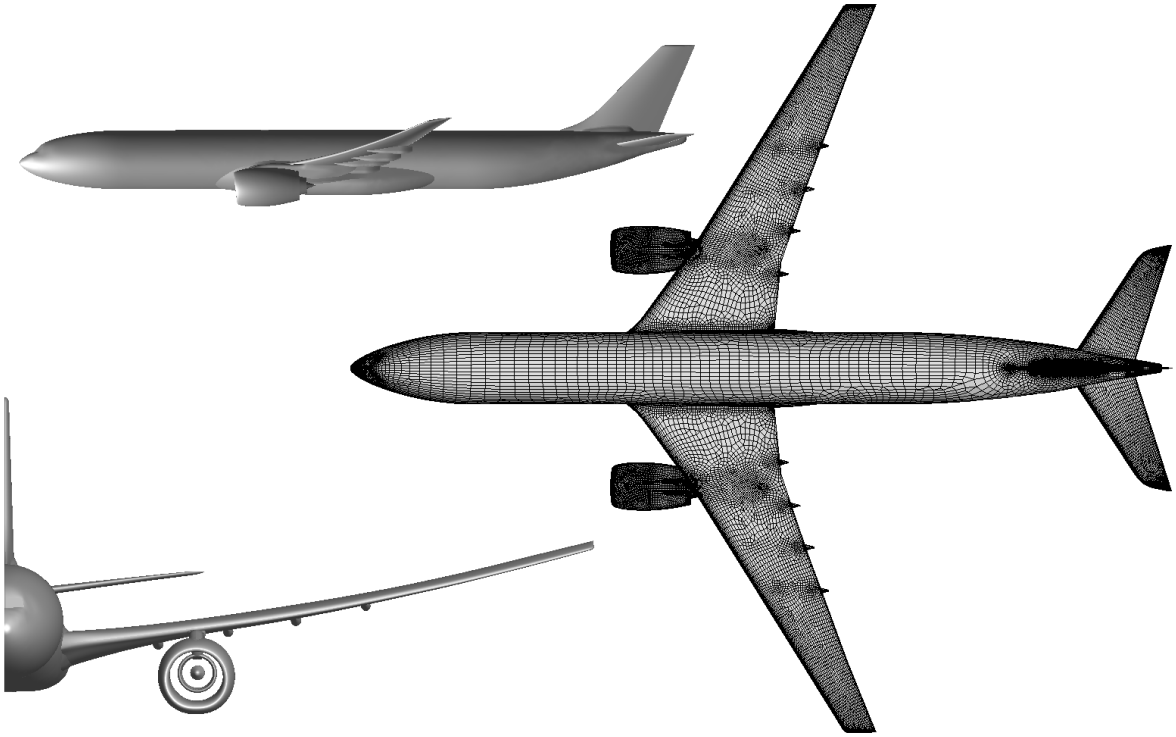

Figure 7: Three-view of XRF1 aircraft and surface mesh.

surface effectiveness from the low-fidelity method which can be seen when comparing the flap angles during the unsteady simulations in Figure 5(b).

Both controllers are now applied to suppress the lift coefficient response for several 1–cos gusts. As defined by international certification requirements, the non-dimensional gust length varies between 2.8 and 35 and the gust amplitude is adjusted accordingly. Resulting combinations of gust length and amplitude are shown in Figure 6(a). The maximum lift coefficient value is extracted from all simulations and given in Figure 6(b) for the uncontrolled, the RANS LFD-based controlled and the DLM-based controlled system response. While both controllers decrease the maximum lift coefficient, the LFD-based controller is significantly more effective and barely shows any deviations from zero.

3.2 Large Passenger Aircraft XRF1

The second investigated test case is the passenger aircraft configuration XRF1, a three-view illustration of which is offered in Figure 7. The XRF1 research test case is used by Airbus to engage with external partners on development and demonstration of relevant capabilities. XRF1 is an industrial standard multidisciplinary research test case representing a typical configuration for a long-range, wide-body aircraft. It features a total mass of about 200,000 kg and a fuselage length-to-diameter ratio of about 11. The wing has the following approximate planform parameters; an aspect ratio of about 8.5, a taper ratio of 0.22 and a 30° quarter-chord sweep angle. The mean aerodynamic chord of the model is approximately 7.5 m with a span and reference area of 57 m and 380 m^2, respectively. Engine nacelles are treated as flow-through.

In contrast to the aerofoil case, the proposed aircraft control system aims at negating the increase in lift coefficient while simultaneously trying to retain a trimmed condition

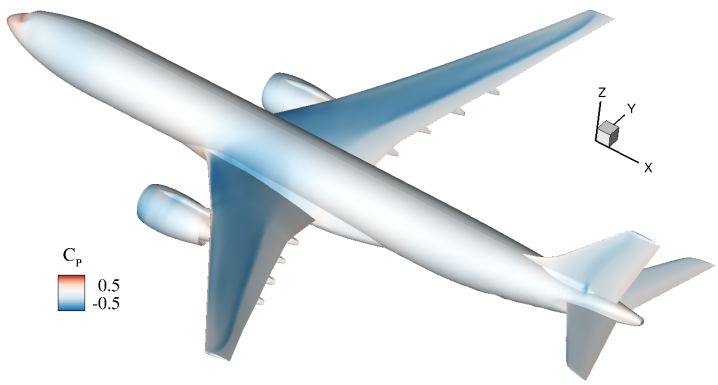

Figure 8: Steady-state surface pressure distribution of XRF1 aircraft.

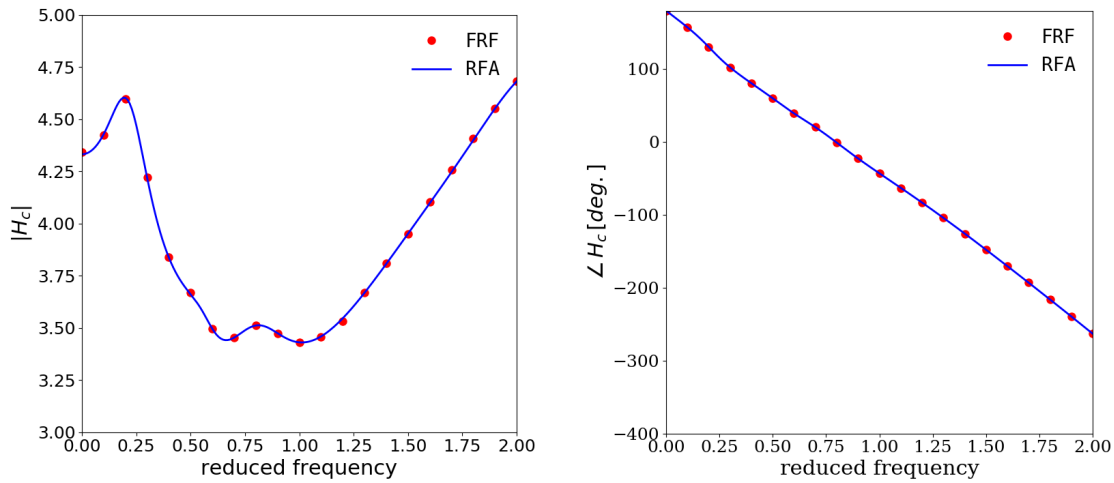

(a) Aileron magnitude

(b) Aileron phase

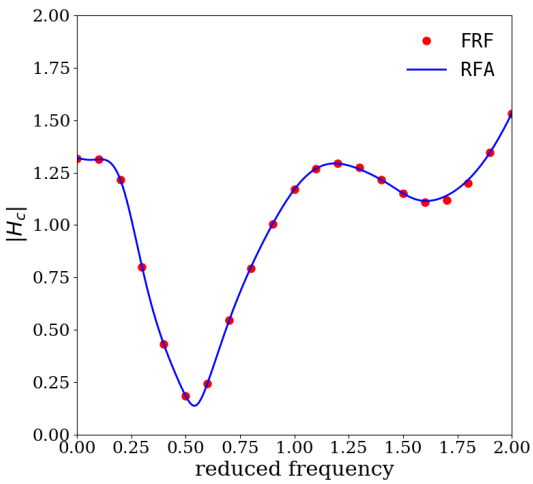

(c) Elevator magnitude

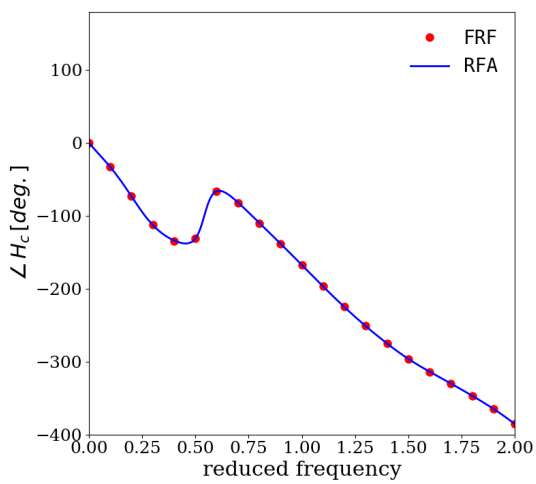

(d) Elevator phase

Figure 9: Frequency response function H_c and its rational function approximation for aileron and elevator of XRF1 aircraft.

with a pitching moment of zero. Therefore, two each of ailerons and elevators, the port side of which are displayed in Figure 2, are used as control surfaces. The ailerons have a length of about 20% semi-wingspan each and the hinge axis it located at 66% chord length. Elevators span across roughly 85% of the horizontal tail plane and their hinge

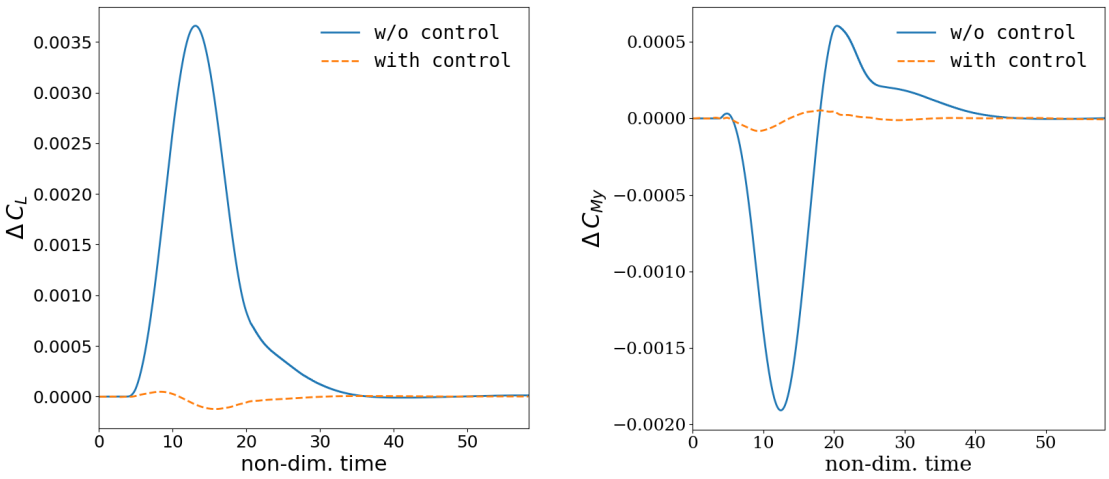

(a) Lift coefficient response

(b) Pitching moment coefficient response

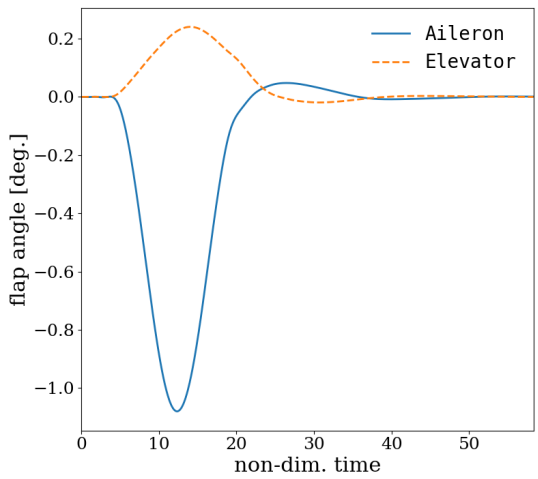

(c) Aileron and elevator deflection angle

Figure 10: Aircraft results with and without control for gust length of 116 m.

axis is at approximately 75% chord length. All control surfaces are modelled as a blended surface without a gap and, as for the aerofoil case, mesh deformation techniques are applied during the RANS simulations. As a prerequisite for unsteady time-marching and frequency-domain simulations, a steady aeroelastic trimming is performed to ensure that lift equals weight and no pitching moment is present at a Mach number of 0.85 and an altitude of 10 km. As described in [15], an artificial horizontal tail plane mode is also defined for trimming purposes. The resulting steady-state surface pressure distribution is shown in Figure 8 and contains a strong shock at roughly 70% chord length, the location of which approximately coincides with the hinge axis of the ailerons.

The FRF of the control law's two components, which account for the aerodynamic response due to the gust and the control-surface deflection, are shown in Figure 9. Whereas the phase angle for the aileron shows a linear decrease with increasing reduced frequency, strongly non-linear behaviour is observed for the magnitude. This could result from the dynamics of the shock in the vicinity of the hinge of the aileron. Recalling that the entries of the FRF given by function H_c describe the transfer between the gust excitation and a control-surface deflection, a relatively large factor of more than 4.5 can be ob-

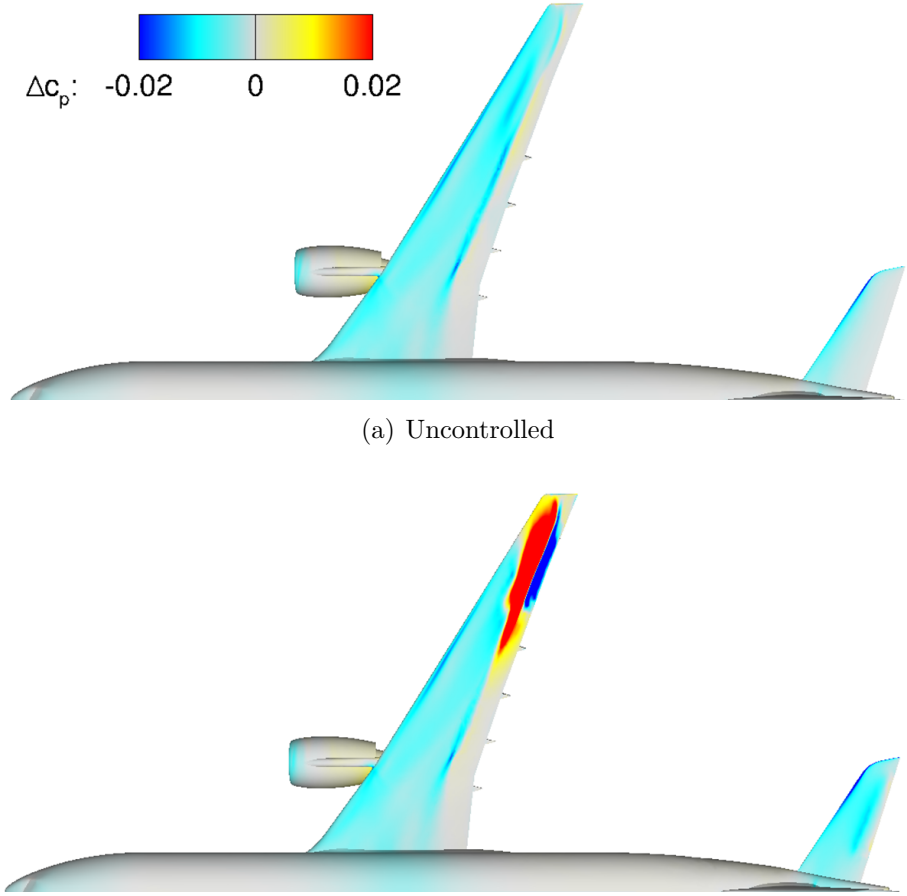

(a) Uncontrolled

(b) Controlled

Figure 11: Aircraft surface pressure distribution at $C_{L,max}$ for gust length of 116 m

served already in the magnitude of the FRF for the aileron, see Figure 9(a) and compare with Figure 4(a). This will result in large control-surface deflections for realistic gust amplitudes. In contrast to the aerofoil case, the area of the ailerons is relatively small compared to the overall wing area and thus its influence on the lift coefficient is significantly smaller. Therefore, using only the generic outer ailerons is not enough to alleviate the gust and additional control surfaces, e.g. inner aileron or spoilers, are required. The approximation using RFA, necessary for a continuous time-domain representation, is also provided showing an excellent agreement with the reference data throughout.

Results of lift and pitching moment coefficient response with and without control law, simulating a 1–cos gust response with a medium gust length of 116 m and a small amplitude of 0.1% of the freestream velocity, are shown in Figure 10. Significant reductions in lift build-up are achieved by the controller nearly eradicating the gust influence on the global integrated coefficients. Aileron deflections up to -1.0 deg are necessary to compensate for the lift build-up directly reflecting the aforementioned trends of the control law magnitude. Note that rigid body motions and elastic deformations are not accounted for in this study and might enhance the effectiveness of the control law since these additional degrees of freedom will withdraw energy from the gust excitation. Moreover, practical constraints of the control devices, such as response time and maximum deflection angles, are currently not accounted for. Thus, to completely compensate the lift coefficient increase encountered during gusts with amplitudes defined by certification re-

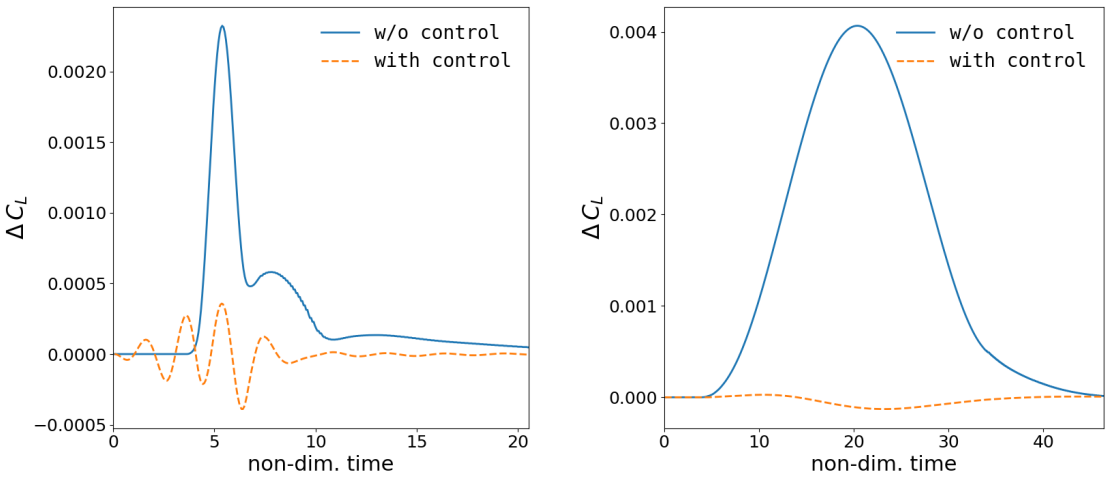

(a) Gust length of 17 m

(b) Gust length of 214 m

Figure 12: Aircraft lift coefficient response with and without control for gust lengths of 17 and 214 m.

quirements (approximately 6% of the freestream velocity), more than ailerons are needed since aileron deflection angles of around 60° are infeasible.

A more detailed analysis of the alleviated gust response for a gust length of 116 m is provided by extracting surface pressure distributions at the time instance of maximum lift coefficient (non-dimensional time of about 15). Results are shown in Figure 11. Due to the upwards deflection of the ailerons, the aerofoil camber is reduced and circulation around the affected wing sections is lowered. Consequently, an upstream shock movement results, while the shock intensity decreases, and the local pressure coefficient increases. Hence, the total lift coefficient remains nearly unchanged even though inboard wing sections produce significantly more lift compared to the undisturbed flow field shown in Figure 8. The elevator deflection causes only a slight additional pressure deviation on the horizontal tail plane due to the significantly smaller deflection of 0.2°, cf. Fig. 10(c).

Finally, the control law is applied to two different 1–cos gusts with gust lengths of 17 and 214 m, respectively. Corresponding lift coefficient responses are shown in Figure 12. While for the longer gust a nearly perfect response (i.e. no significant increase in lift) is obtained, the shorter gust length features several oscillations before and during the aircraft-gust interaction. This results from the limited frequency sampling range up to a value of 2.0. Previous studies have shown that for shorter gusts reduced frequencies at least up to 3.0 should be pre-computed [15]. Without those support points, the fifth-order polynomial used for the RFA introduces large deviations outside the sampling range, which ultimately leads to oscillations in the aerodynamic response.

4 CONCLUSIONS

Sizing for gust loads is an integral part of aircraft design. Higher-fidelity computational fluid dynamics, specifically linearised methods, have matured in recent years to be used routinely in the industrial process for aircraft loads and aeroelastics. However, such methods are rarely used in control law design for active gust load alleviation. Hence, this work presents first results of using higher-fidelity aerodynamics in designing a simple gust controller aimed at negating gust-induced loads via deploying conventional control surfaces. Following a demonstration for a transonic aerofoil case, the methods are successfully ap-

plied to a close-to-production large civil aircraft. Overall, it is expected that current control law design based on linear-potential aerodynamic theory can be readily enhanced when using equivalent computational fluid dynamics methods.

ACKNOWLEDGMENT

The authors would like to thank Airbus for providing the XRF1 test case as a mechanism for demonstration of the approaches presented in this paper.

REFERENCES

[1] Kopf, M., Bullinger, R., Giesseler, H.-G., et al. (2018). Model Predictive Control for Aircraft Load Alleviation: Opportunities and Challenges. In *2018 Annual American Control Conference(ACC)*.

[2] Albano, E. and Rodden, W. P. (1969). A Doublet Lattice Method for Calculating Lift Distribution on Oscillating Surfaces in Subsonic Flow. *AIAA Journal*, 7(2), 279–285.

[3] Regan, C. D. and Jutte, C. V. (2012). Survey of applications of active control technology for gust alleviation and new challenges for lighter-weight aircraft. Tech. Rep. NASA/TM-2012-216008, NASA.

[4] Liu, X. and Sun, Q. (2016). Gust Load Alleviation with Robust Control for a Flexible Wing. *Shock and Vibration*, 2016. Article ID 1060574.

[5] Zhao, Y., Yue, C., and Hu, H. (2016). Gust Load Alleviation on a Large Transport Airplane. *Journal of Aircraft*, 53(6), 1932–1946.

[6] Raveh, D. E. (2007). CFD-Based Models of Aerodynamic Gust Response. *Journal of Aircraft*, 44(3), 888–897.

[7] Wales, C., Jones, D., and Gaitonde, A. (2015). Prescribed Velocity Method for Simulation of Aerofoil Gust Responses. *Journal of Aircraft*, 64–76.

[8] Reimer, L., Ritter, M., Heinrich, R., et al. (2015). CFD-based Gust Load Analysis for a Free-flying Flexible Passenger Aircraft in Comparison to a DLM-based Approach. In *22nd AIAA Computational Fluid Dynamics Conference*. AIAA 2015-2455.

[9] Clark, W. S. and Hall, K. C. (2000). A Time-Linearized Navier-Stokes Analysis of Stall Flutter. *Journal of Turbomachinery*, 122(3), 467–476.

[10] Widhalm, M., Dwight, R. P., Thormann, R., et al. (2010). Efficient Computation of Dynamic Stability Data with a Linearized Frequency Domain Solver. In *5th European Conference on Computational Fluid Dynamics*. ECCOMAS CFD 2010.

[11] Pechloff, A. and Laschka, B. (2010). Small Disturbance Navier-Stokes Computations for Low-Aspect-Ratio Wing Pitching Oscillations. *Journal of Aircraft*, 47(3), 737–753.

[12] Thormann, R. and Widhalm, M. (2013). Linear-Frequency-Domain Predictions of Dynamic-Response Data for Viscous Transonic Flows. *AIAA Journal*, 51(11), 2540–2557.

[13] Kaiser, C., Thormann, R., Dimitrov, D., et al. (2015). Time-Linearized Analysis of Motion-Induced and Gust-Induced Airloads with the DLR TAU Code. In *Deutscher Luft- und Raumfahrtkongress*.

[14] Förster, M. and Breitsamter, C. (2015). Aeroelastic Prediction of Discrete Gust Loads Using Nonlinear and Time-Linearized CFD-Methods. *Journal of Aeroelasticity and Structural Dynamics*, 3(3), 252–255.

[15] Bekemeyer, P., Thormann, R., and Timme, S. (2017). Frequency-Domain Gust Response Simulation using Computational Fluid Dynamics. *AIAA Journal*, 55(7), 2174–2185.

[16] Timme, S. and Thormann, R. (2016). Towards Three-Dimensional Global Stability Analysis of Transonic Shock Buffet. In *16th AIAA Aviation Technology*. AIAA 2016-3848.

[17] Belesiotis–Kataras, P. and Timme, S. (2018). Numerical Study of Incipient Transonic Shock Buffet on Large Civil Aircraft Wings. In *Royal Aeronautical Society 2018 Applied Aerodynamics Conference*.

[18] Reimer, L. (2015). The FlowSimulator - A software framework for CFD-related multidisciplinary simulations. In *European NAFEMS Conference Computational Fluid Dynamics (CFD) – Beyond the Solve*.

[19] Schwamborn, D., Gerhold, T., and Heinrich, R. (2006). The DLR TAU-Code: Recent Applications in Research and Industry. In *European Conference on Computational Fluid Dynamics*. ECCOMAS CFD 2006.

[20] Stickan, B., Dillinger, J., and Schewe, G. (2014). Computational aeroelastic investigation of a transonic limit-cycle-oscillation experiment at a transport aircraft wing model. *Journal of Fluids and Structures*, 49, 223–241.

[21] Neumann, J. and Mai, H. (2013). Gust response: Simulation of an Aeroelastic Experiment by a Fluid-Structure Interaction Method. *Journal of Fluids and Structures*, 38, 290–302.

[22] Dwight, R. (2006). An Implicit LU-SGS Scheme for Finite-Volume Discretizations of the Navier-Stokes Equations on Hybrid Grids. *DLR-FB-2005-05*.

[23] Michler, A. (2011). Aircraft control surface deflection using RBF-based mesh deformation. *International Journal for Numerical Methods in Engineering*, 88, 986–1007.

[24] Parameswaran, V. and Baeder, J. D. (1997). Indicial Aerodynamics in Compressible Flow-Direct Computational Fluid Dynamic Calculations. *Journal of Aircraft*, 34(1), 131–133.

[25] Xu, S., Timme, S., and Badcock, K. J. (2016). Enabling off-design linearised aerodynamics analysis using Krylov subspace recycling technique. *Computers and Fluids*, 140, 385–396.

[26] Saad, Y. (2003). *Iterative Methods for Sparse Linear Systems*. Philadelphia, PA: Society for Industrial and Applied Mathematics, 2nd ed. ISBN 0898715342.

COPYRIGHT STATEMENT

The authors confirm that they, and/or their company or organization, hold copyright on all of the original material included in this paper. The authors also confirm that they have obtained permission, from the copyright holder of any third party material included in this paper, to publish it as part of their paper. The authors confirm that they give permission, or have obtained permission from the copyright holder of this paper, for the publication and distribution of this paper as part of the IFASD-2019 proceedings or as individual off-prints from the proceedings.